ELSEVIER

Contents lists available at ScienceDirect

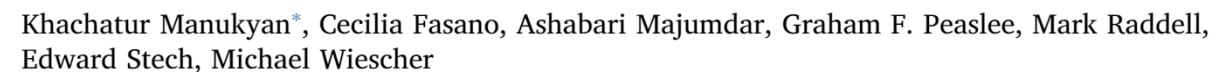
# **Applied Surface Science**

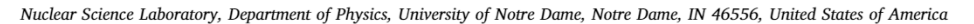
journal homepage: www.elsevier.com/locate/apsusc



Full length article

## Surface manipulation techniques of Roman denarii







ARTICLE INFO

Keywords: Silver-copper alloy Roman coin X-ray fluorescence Particle-induced X-ray emission Electron microscopy

#### ABSTRACT

This work presents results of macro, micro, and nanoscale surface characterization for a set of Roman denarii, ranging from 136 BCE to 240 CE, using large-scale X-ray fluorescence (XRF) mapping, particle-induced X-ray emission (PIXE) spectroscopy, focused-ion-beam-assisted scanning electron microscopy (FIB-SEM) with energy dispersive spectroscopy (EDS). The combination of XRF and PIXE, with varying beam energies, allowed for visualization and quantification of individual elements as a function of the surface distribution. These results helped to select suitable areas for FIB-SEM-EDS analysis. The edges of selected coins were polished to image the inner composition and surface morphology of the coins using a backscattering electron (BSE) imaging method and EDS mapping. Nanosized lamellas extracted from the coins were investigated by transmission electron microscopy (TEM) as well. The combination of these methods enabled the surface, the subsurface, and volume composition of these coins to be probed to better understand their production methods, their surface treatment methods, and their corrosion. The results also provide evidence that a particular surface treatment method, amalgam silvering, had been used to make authentic Roman coins as early as the third century CE.

#### 1. Introduction

Accurate characterization of metallic artifacts, such as coins, provides essential information for archeologists and historians which when combined with the known dates of production helps them to understand the technology of preparation, circulation patterns over time, and the best way to manage conservation and restoration [1-8]. One of the most significant artifacts of the ancient world is the Rome denarius [9,10]. This silver coin was introduced in the second century BCE after the Punic Wars as the official currency of the Republic. Romans minted denarii from silver alloy with an original standard of 72 Denarii (~4.5 g) from one Roman pound of silver (328.5 g) [9]. Denarii helped finance the expansion of the Republic and the civil wars of the first century BCE. During the civil wars, devaluation occurred by gradually reducing the weight to  $\sim 3.8$  g per coin [9,10]. This value was established as a new standard with the currency reform of Emperor Augustus. The denarius was then used as the standard currency for the first 250 years of the Roman Empire.

The debasement of the denarius by increasing copper content, or sometimes by the use of lead and tin, was accompanied by the development of surface modification approaches to ensure that the coins would look similar to pure silver [9–13]. One technique that was used to manipulate the surface composition of silver alloys, which is still

used by modern silver coin producers, involved heating the Ag—Cu alloy in the air to oxidize Cu at the surface. The heat-treated coin blanks were then soaked in dilute organic acid, such as vinegar (acetic acid), to dissolve out copper from the surface of the alloy. This method created a copper depleted, porous layer of pure silver on the surface of the coin and could have kept the public unaware of the debasement.

Inverse segregation may have been another method for coin surface enrichment of silver. Modern laboratory experiments suggest a natural segregation process during the solidification of Ag–Cu alloys which results in an Ag-rich layer of  $\sim\!20\,\mu m$ , while the bulk alloy has a lower silver content [14]. Such a segregation process can only be performed under slow solidification conditions. The Ag-rich layer formation was probably difficult to achieve in Roman mints. Some archeological evidence suggests that molten silver alloy was cast in stone molds, which would increase the cooling rate and thus decrease the time needed for slow inverse segregation [14].

Romans also used the mechanical joining of thin silver foils to debased alloy blanks by hammering or by using tin as soldering material [1,15]. Another method for alloy surface manipulation was amalgam plating. This method allowed metalsmiths to place a thin layer of noble metal on top of a substrate. Mercury plating of silver, amalgam silvering, was done in the same way as gilding. Workers would apply a viscose paste of Hg - Ag on a substrate and then heat the system to

E-mail address: kmanukya@nd.edu (K. Manukyan).

<sup>\*</sup> Corresponding author.

induce a diffusion bond between the substrate and the newly formed layer. They would then heat the coin again to evaporate excess mercury [15]. This technique was a common practice for silvering harnesses, belt fittings, heraldic pendants, counterfeit coins, and other objects in medieval Europe [15]. The use of amalgam silvering in the Roman empire is a matter of debate [4,8,16,17]. There is an opinion among many historians that during the later periods of the Roman empire, a complex alloy (with a silver content of only 5%) was plated with a thin silver coating which wore off quickly during circulation [9]. Recently reported analytical results showed that this widely held belief might not be true because even during a crisis period within the Empire (249 to 274 CE), Romans produced high-quality coinage [4]. This study also identified a coin dating back between 270 and 275 CE that contained a thin (corroded) silver layer with traces of mercury suggesting that amalgam silvering was used to manipulate the surface of coins [4].

Despite significant advances that have been achieved in the characterization of metal artifacts, minting preparation steps and methods of surface manipulation in coins are still not comprehensively understood. The historical value of these artifacts requires the use of nondestructive techniques such as neutron activation analysis (NAA), X-ray fluorescence (XRF) and particle induced X-ray emission (PIXE). NAA measures the isotopic composition of the entire coin but returns an incorrect estimation because the analysis represents the average of the surface and bulk compositions [18,19]. XRF and PIXE provide rapid analysis of the surface elemental composition of alloys [2,20-26]. The maximum sampling depth (~100  $\mu m)$  for PIXE is limited by the energy of the proton beams used. Higher beam energies (above 5 MeV) would activate the copper through nuclear reactions and would, therefore, require extended post-analysis storage while the induced activity of the samples decays [27]. XRF provides similar information with deeper probing depth ( $\sim$ 250–350 µm) for Ag–Cu alloys [28].

Laser ablation inductively coupled mass spectroscopy (LA-ICP) is a micro-destructive method that produces a reliable elemental analysis to determine the surface chemical composition of coins [11,29,30]. The maximum sampling depth for LA-ICP is limited to  $\sim\!50\,\mu m$ . Focused ion beam (FIB) milling combined with scanning electron microscopy (SEM) is another micro-destructive surface characterization method. This method, coupled with energy-dispersive X-ray spectroscopy (EDS), allows for the determination of the composition and microstructure of coins at the maximum surface layer of  $\sim\!50\,\mu m$  [4]. Destructive metallographic analysis using optical or electron microscopy provides complete information for revealing fabrication and surface modification techniques of coins [12,13,31,32].

In this work, several of these surface characterization methods are combined to bridge the gaps in specific techniques. Large-scale XRF mapping, PIXE, FIB-SEM, TEM, and high-resolution EDS are all used to characterize a set of Denarii from different periods between 136 BCE and 240 CE (Fig. 1). Combining of localized spot analysis, using XRF mapping and PIXE, of varying proton beam energies allowed us to visualize the surface distribution of individual elements. These results guided the selection of suitable regions for further FIB-SEM and EDS analysis. The edges of selected coins were polished to remove a layer, with a thickness of 1 to 3 mm, that could be imaged with the backscattering electron (BSE) and EDS elemental mapping methods. Thin (~100 nm) lamellas lifted out from the surface of coins were also investigated by transmission electron microscopy (TEM) to reveal the composition and structure of coins at the nanoscale. These methods allowed investigation of the surface, subsurface, and bulk composition of the coins which revealed some aspects of manufacturing methods as well as degradation patterns. The results also disclose some surface treatment methods of the coins, including new evidence of the use of amalgam silvering during the early third century.

#### 2. Experimental

#### 2.1. Coins and calibration standards

Twenty (19 Denarii and 1 Antoninianus) coins, drawn from a private collection, minted between 136 BCE and 240 CE (Fig. 1) were investigated. Two Netherland silver, 1 Gulden coins with 94.5% (minted in 1914) and 72.0% (minted in 1928) nominal silver content were used as calibration standards for XRF and PIXE measurements. These calibration coins were polished on both sides, and the edges were trimmed to remove ~1 mm of the surface layer. A small sample was taken from the center of cut coins and dissolved in nitric acid to analyze Ag and Cu content by inductively coupled plasma (ICP) with atomic emission spectrometry (AES) using a Perkin Elmer Optima 8000. The measurements of the elements were made with the instrument default parameters (viewing height 15 mm, nebulizer flow 1.000 l/min, plasma power 1000 W, auxiliary gas flow 1.0 l/min, and plasma gas flow 15 l/ min). The wavelengths of 328.068 nm and 324.754 nm were used to analyze silver and copper, respectively. The standard stock solutions (Merck) of Ag and Cu (1000 mg/l) for the ICP-AES measurements were used to obtain calibration curves. The working concentration of solutions ranged from 1 to 15 mg/l. ICP-AES analysis confirmed nominal Ag, as well as allowing for the determination of the Cu content in both coins. These polished Guldens were used as the standard for other investigations along with ASTM B742 silver 99.90% standard.

#### 2.2. XRF and PIXE analysis

EDAX Orbis PS micro-XRF with a ruthenium X-ray tube (50 kV and 50 W) and ultra-high intensity poly-capillary optics were utilized for elemental analysis. The analyzer is equipped with an automated primary beam filter system, 30 mm<sup>2</sup> silicon drift detector, a dual color CCD camera  $(3 \times, 10 \times \text{ and } 75 \times \text{ digital zoom})$  and a sample stage with automated XYZ positioner. The focusing and collimating X-ray optics system allowed improved detection limits through reduction of Bremsstrahlung scatter, removal of tube characteristic lines, and elimination of Bragg diffraction. The system is capable of producing a focused X-ray beam with a spot size of ~30 μm. In a typical mapping experiment, a coin was attached to the stage, the chamber was evacuated with a pump to ~ 6 Pa pressure, and the analyzer was set to automatic mapping mode. The experimental conditions for scanning were 40 keV, 300 mA, and 0.3 s sampling time per spot. The distance between spots was 20 µm. Orbis Vision software was used to process high-resolution two-dimensional elemental maps. After acquiring maps, the X-ray beam with 2 mm in diameter and 40 keV energy was used to analyze at least ten spots on each coin.

The PIXE experiments were performed on two different NEC Pelletron® tandem accelerators at the Nuclear Science Laboratory at the University of Notre Dame. Proton beams with an energy of 3.4 MeV and intensities of  $\sim 50\,\text{nA}$  and were used to penetrate a  $\sim 8\,\mu\text{m}$  thick Kaptan® window to impinge on the coins mounted ~2.0 cm from the exit window. The X-rays were detected using an Amptek XR-100 silicon drift detector, with a  $\sim 130 \, \mu m$  Be window and  $25 \, mm^2$  active area positioned at a 65° backward angle with respect to the beam. In addition,  $\sim$ 5 nA of 7 MeV protons were used to penetrate through a  $\sim$ 6  $\mu m$ thick aluminized mylar window to probe the coins, which were positioned at a distance of 2.6 cm from this exit window. The X-rays were analyzed using an Ortec SLP Series Lithium-Drifted Silicon detector with a ~130 μm Be window, and an active diameter of 79 mm<sup>2</sup> positioned at a 40° backward angle to the beam direction. The X-ray spectra were characterized by the  $K_{\alpha}$  and  $K_{\beta}$  transitions from Ag and Cu as well as other elements (Fe, Au, Br, Hg, Pb, Bi). The spectra were analyzed using GUPIX software [33].



Fig. 1. Photos of Roman coins from the republican to the imperial periods characterized. D - Denarii, A - Antoninianus: Date are approximate.

## 2.3. Phase composition and microstructure investigations

The phase composition of coins' surfaces was determined by X-ray diffraction (XRD) analysis with Ni-filtered Cu-K $_{\alpha}$  radiation (D8 Advance, Bruker) operated at 40 keV and 40 mA. Step-scan data (of step size  $0.02^{\circ}$  and counting time 4 s) of coins was recorded over the angular range  $2\theta=20-80^{\circ}$ .

Microstructures of two polished coins were examined with a field emission scanning electron microscope (Magellan 400) equipped with a Bruker EDS analyzer. A Helios NanoLab600 system (FEI) with dual electron/ion beam was used to produce cross-sections on coins by ion milling with a gallium ion beam. First, a  $0.3\,\mu m$  thick layer of platinum in a  $10\,\mu m \times 0.5\,\mu m$  rectangular area was deposited onto the selected particle of ball milled material. Next,  $\sim\!50\,\mu m$  deep trench with  $45^\circ$  base angle was milled on the surface under an accelerating voltage of 5 keV and a milling current of 27 nA. Then, a 40 nm thick layer was milled in the side wall of the trench under an accelerating voltage of 5 keV and a milling current of 700 pA to produce a clean cross-section without milling artifacts. After that, the electron-beam was used to image the side wall of the trench at an angle of  $52^\circ$  from parallel to the side wall.

The TEM samples were also prepared using a Helios NanoLab 600 system by making cross-sectional slices from top surfaces of coins. Darkfield and scanning TEM imaging, along with electron diffraction analysis, were performed with an FEI-Titan 80–300 transmission electron microscope (TEM) at 300 keV. The chemical composition of the TEM samples was characterized by high-resolution EDS (INCA, Oxford Instruments).

#### 3. Results and discussions

#### 3.1. Micro-XRF mapping

Fig. 2 illustrates color-coded XRF elemental distribution maps and their overlays for three coins. The intensity of each color is associated with the relative quantity of analyzed elements within the  $10-20\,\mu m$  surface layer of the coin. The maps of coin D2 exhibit non-uniform elemental distribution. Table 1 summarizes the elemental composition of different areas analyzed by a 1 mm X-ray beam spot. Such single-spot XRF analyses indicate that the areas marked a1, and a3 on the overlay image contain a significant amount of copper and iron, along with

silicon and calcium. Such a composition suggests the presence of slag, an oxide by-product of metal smelting. The presence of Fe and the other elements could also be related to the interaction between the coin and the burial soil components. Color overlay image shows that the layer attached to the surface of coin accelerated the pitting corrosion and selectively enriched the quantity of Cu at specific regions. The areas marked a2 and a4 on the overlay image contain Ag as the significant element along with Fe, Cu, and S (Table 1). Ag<sub>2</sub>S is a black tarnish layer known to form on coins through the reaction of silver with sulfur. The overlay image shows that sulfur concentration increases toward the edges of the coin, which is most likely due to the structural imperfections. The elemental maps (Fig. 2) for coins D7 and D10 exhibit similar trend with higher sulfur content at the areas of the minted letters (b1 and c1), as compared to flat regions (b2 and c2). The overlay image for D7 coin indicates areas with elevated amounts of bromine (b1, b4). The presence of bromine on the surface could be associated with exposure to marine water [34]. This coin also contains some silicon and aluminum (Table 1). Large copper enriched regions, such as one marked as b2, can also be seen on the overlay image. The local single-spot analysis shows no lead or gold on this coin as compared to D2 coin (Table 1). Distribution of metals on D10 coin is more uniform. This coin contains small amounts of Au and Pb (Table 1). However, the XRF mapping indicates the presence of Si presumably as part of slag attached on the surface, along Ca, Al, Fe, and Ti, identified by the single-spot analysis.

Fig. 3 shows another dataset of the micro-XRF mapping of investigated coins. These qualitative results indicate that the silver is the primary element on the surfaces of coins minted during the Roman Republic and the first two centuries of the Roman empire (D1, D4, D5, and D11). The metal distribution on coin D11 is non-uniform. The surface distribution of metals on coins struck during the reign of Severan Emperors (D13 and D15) is also non-uniform and consists of both Ag- and Cu-rich areas. The Ag content for the D16 coin minted at 213 CE (Caracalla) shows much higher silver content compared to the previous two samples. The surface of the D19 coin also shows significant non-uniformity with both Cu- and Ag-rich regions.

Micro-XRF elemental mapping also indicates that the Fe is present on early coins. Chlorine content is significantly higher on the surface of D3 and D4 coins minted during the reigns of Tiberius and Nero, respectively. The distribution of Cl, however, is non-uniform and concentrated at uneven areas. The D4 coins show more uniform chlorine

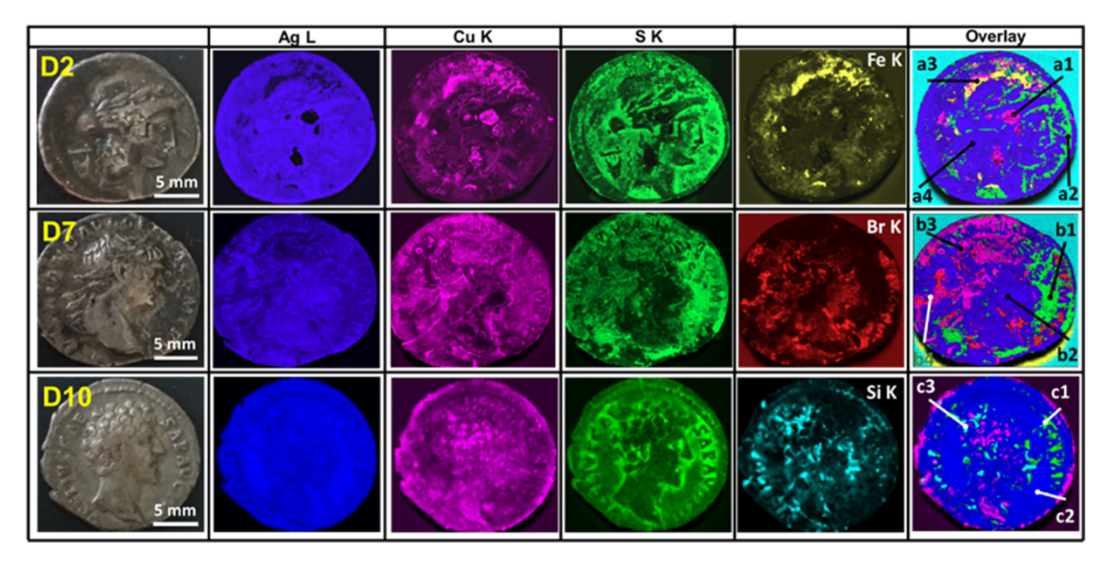


Fig. 2. Maps for selected elements and their color overlays obtained by micro-XRF scanning.

distribution across the surface. The sulfur content on the coins' surface shows a correlation with silver. The areas with more silver exhibit higher sulfur content. Results of large scale micro-XRF mapping shown in Figs. 2 and 3 helped to identify the areas for further quantitive analysis and allowed for the avoidance of corroded regions, which do not represent the original alloy composition accurately.

#### 3.2. XRF and PIXE analysis of copper content

Guided by micro-XRF mapping, additional single-spot PIXE, and XRF analysis was conducted. In the latter case, the X-ray beam with 2 mm in diameter and 40 keV energy was used to analyze at least ten spots on each coin. These measurements allowed analysis of elemental surface composition with a sampling depth of ~250µm. PIXE complemented XRF analysis using a proton with an energy of either 7 MeV (2 mm proton beam diameter) or 3.4 MeV (8 mm proton beam diameter). The sampling depths for these measurements were ~140 and ~50 µm, respectively. Thus, using XRF and PIXE with different energies allowed for depth profiling of elemental composition. Fig. 4 shows the average copper content for each coin measured by both XRF and PIXE as a function of time. The results indicate that copper content on the surfaces of D1 through D4 coins is low, and increasing the sampling depth weakly influenced its reported content. The results suggest that the coins were minted using low copper content alloys and surface modification efforts were minimal. These data also demonstrate the stability of Roman silver coinage during the period of the Republic despite the economic difficulties and the civil wars that led to the fall of the republic and the establishment of the Roman Empire. The figure also demonstrates the debasement by Nero in 65 CE (D5) and Trajanus (D8). Cu content depending on sampling depth indicated that debasement was accompanied by a significant surface modification to deplete copper on the coin surface. The rapid increase and fluctuation of copper content at the end of the second century CE and the first 40 years of the third century CE provide evidence for the drastic devaluation policies established under Septimus Severus and his co-rulers (D13–D16) as well as later emperors (D17–D19, A20). Significant differences in copper, depending on sampling depth, for the coins minted in third century CE indicate extensive use of surface modification methods.

#### 3.3. The phase composition of coins

XRD analysis of selected coins was conducted to determine their phase composition. The sampling depth of this analysis depended on alloy composition, X-ray energy, and incident angle limited to the surface layer with approximately  $10\text{--}20\,\mu\text{m}$  thickness. All XRD patterns show strong peaks of the Ag-rich phase ( $\alpha\text{--phase}$ ), while the Cu-rich phase ( $\beta\text{--phase}$ ) can be detected only for some coins (Fig. 5). Two elements in Ag—Cu alloys have low mutual solubility and upon solidification two distinct  $\alpha\text{--}$  and  $\beta\text{--phase}$  separate, according to the biphasic diagram [35]. A small amount of dissolved copper in  $\alpha\text{--phase}$  causes a shift of the diffraction peaks' positions.

In addition to Ag and Cu, the coins minted during the Roman Republic and first century CE contain AgCl, which agrees well with XRF analysis showing chlorine on the surface of these coins. Although XRF analysis indicates some sulfur on the coin surface, no peaks for  $Ag_2S$  can be seen on XRD patterns. Coins minted during the second and third

Table 1
Composition of elements determined by single-spot XRF analysis at selected areas shown in Fig. 2. The X-ray spot size is 1 mm. Experimental error is 2.5–3.5%.

Coin	Area in Fig. 2	Elemental composition, wt%.												
		Ag	Cu	S	Fe	Au	Pb	Si	Ca	Al	Ti	Br		
D2	a1	31.8	32.25	3.43	3.05	2.55	2.55	21.48	2.92					
	a2	85.5	1.76	10.8	0.47	0.82	0.66							
	a3	42.3	18.3	3.9	9.22	1.05	0.68	15.1	9.47					
	a4	98	0.55	0.43	0.1	0.88								
D7	b1	78.3	5.22	7.56	0.08			3.71		2.03		3.11		
	b2	92.4	1.99	1.15				2.91		0.83		0.75		
	b3	79.5	6.1	11.6				2.66				0.21		
	b4	85.3	4.94	5.72				1.34				2.72		
D10	c1	95.2	1.84	1.21	0.1	0.67	0.96							
	c2	95.3	2.55	0.39	0.08	0.52	1.16							
	c3	89.6	2.23	0.23	0.11	0.54	0.65	5.28	0.82	0.11	0.42			

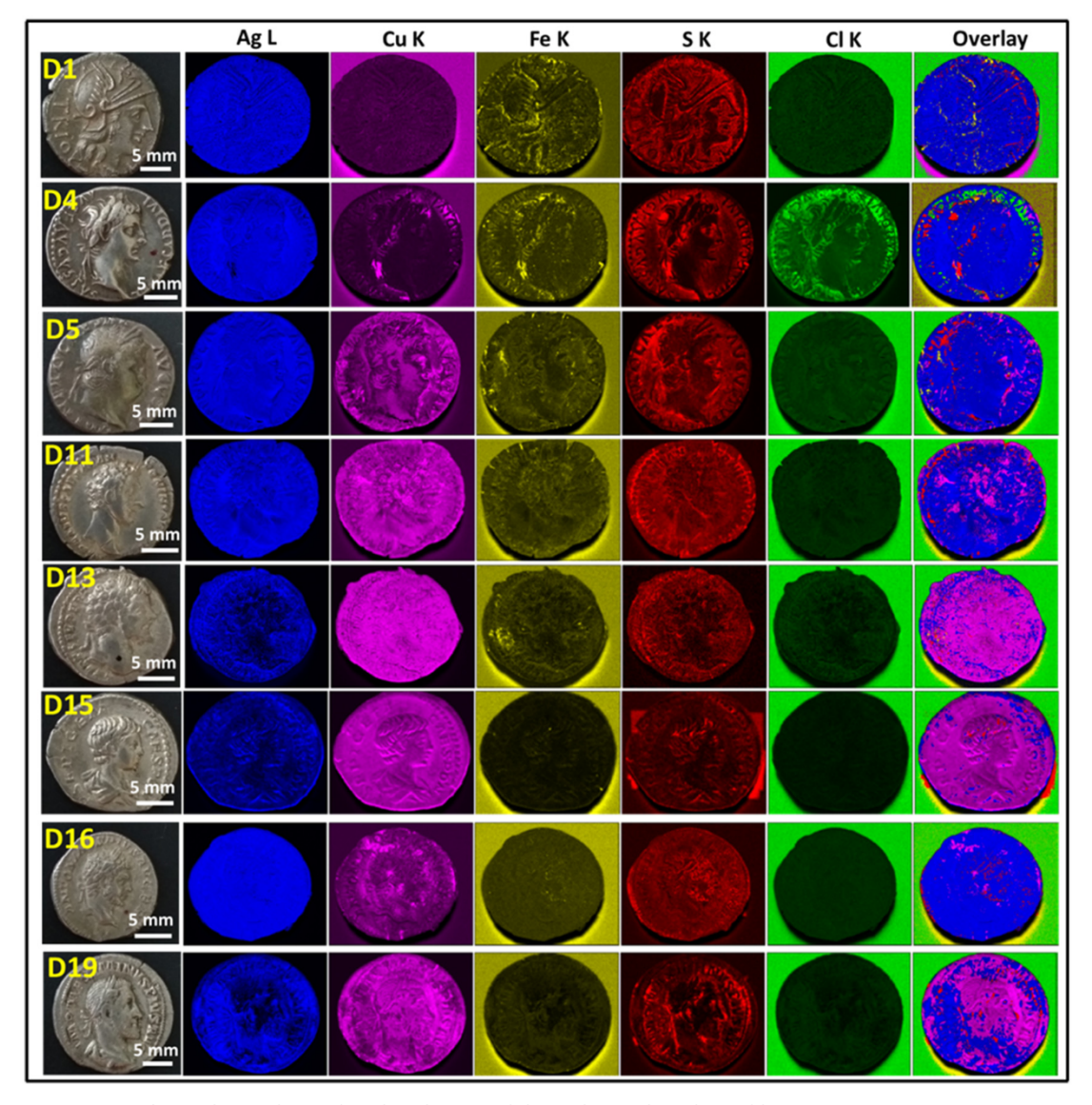


Fig. 3. Elemental maps for selected coins and their color overlays obtained by micro-XRF scanning.

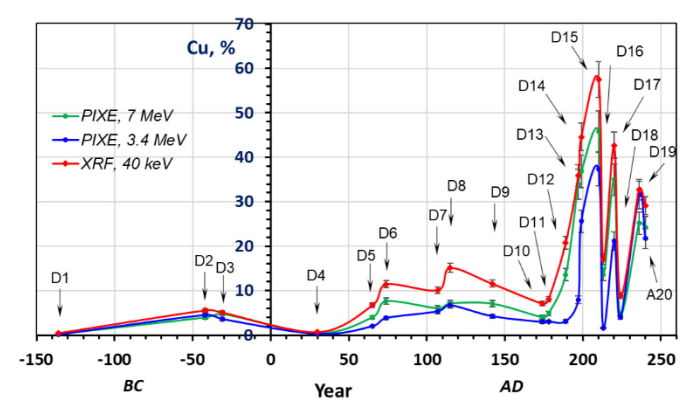


Fig. 4. The measured copper content in the denarii minted during Roman Republic and Empire.

centuries exhibit peaks of Cu-rich  $\beta$ -phase as well as Cu<sub>2</sub>O (copper corrosion product) as a minor surface phase.

To reveal the surface and bulk distribution of  $\alpha$ - and  $\beta$ -phases, the edges of two coins (D16 and D17) were polished to remove a layer with a thickness of 1 to 3 mm to be imaged by back-scattering electron (BSE)

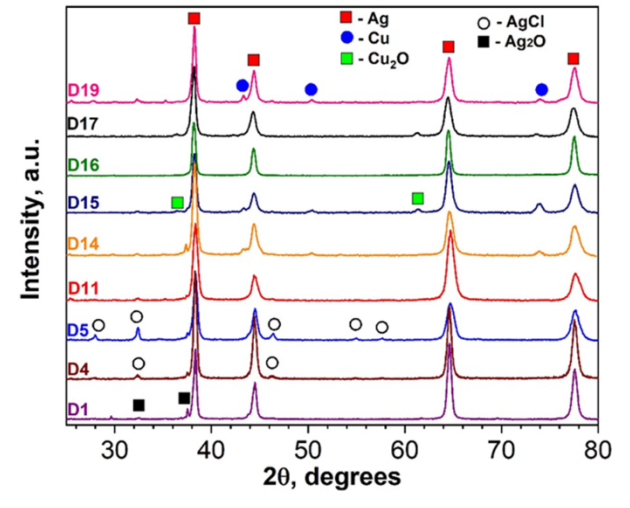


Fig. 5. XRD patterns of selected coins.

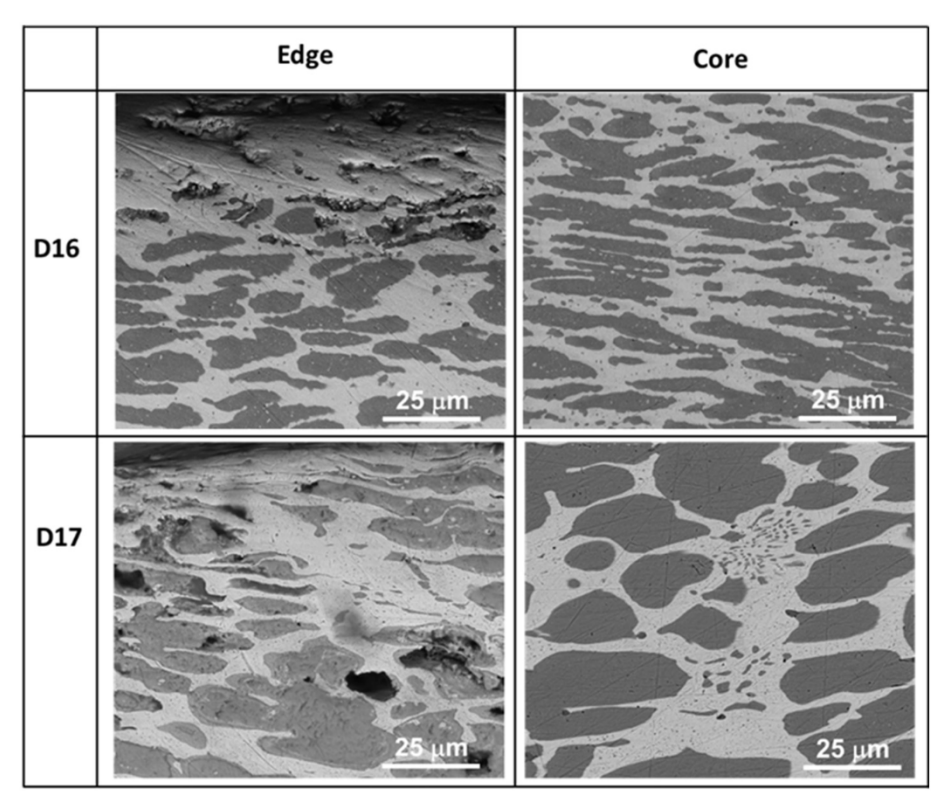


Fig. 6. BSE images of the surface and bulk morphology for two polished coins.

and EDS elemental mapping methods. Both coins have an Ag-rich layer on the surface, which is shown as the lighter phase (higher energy backscattered electrons) from Ag, and the darker grey phase from Cu (Fig. 6). The thickness of the Ag-rich layer for D16 coin is  $\sim 30~\mu m$ , which prevents detection of  $\beta$ -phase by XRD (see Fig. 5, D16 curve). The thinner ( $\sim 10~\mu m$ ) Ag-rich layer on coin D17's surface allows for detection of the  $\beta$ -phase (Fig. 5, D17 curve).

EDS microanalysis of Ag-rich surface layers for both coins shows 85-95% silver with amounts of copper and oxygen as minor constituents. BSE images of the core of both coins illustrate the grains (dendritic) of  $\beta$ -phase (Cu > 92%) surrounded by a eutectic phase (the mixture of both  $\alpha$  and  $\beta$  phases) containing, on average, 72% Ag. BSE images demonstrate that dendritic growth is the primary segregation mechanism that occurred during the casting of these coin blanks. This segregation arises in alloys because one of the constituents usually has a lower melting point than the other. Normal segregation and inverse segregation are other possible processes that can occur during the solidification of Ag-Cu melts. During the normal segregation, the lower melting point phase is concentrated toward the mold core, while in inverse segregation Ag can concentrate to the surface of the mold resulting in the Ag-rich layer. This inverse segregation can be realized in slow cooling conditions, which often were not the case in Roman silver mints.

EDS elemental mapping (Fig. 7) shows that the surfaces of both coins contain oxygen. Oxygen localized at the D16 Ag-rich layer while for the D17 coin, oxygen distributed at both the Ag-rich surface and subsurface regions. Therefore, the presence of oxygen and pores at Agrich surface layers in studied coins can be attributed to the chemical leaching. Copper residues generated after soaking in acidic solutions oxidized to form Cu<sub>2</sub>O surface phase were identified by XRD analysis (Fig. 5).

## 3.4. FIB-SEM-EDS analysis

Destructive metallographic tests presented in the previous section

are the best way to reveal the complete microstructural characteristics of coins. Such an approach, however, is not acceptable for coins with high historical value. FIB-assisted SEM imaging coupled with EDS microanalysis allows exploration of the microstructure and composition of the outer surface (40–50 µm depth) of coins. This combination of techniques helps us to understand the methods that had been used to manipulate the surface of coins as well as revealing the corrosion processes of coins. Fig. 8 and Table 2 present a set of SEM-EDS images of investigated coins and highlight their morphological.

differences. The coins (D1 and D4) minted during the Roman Republic exhibit large (1–5  $\mu m)$  grains and small pores with sizes ranging from 0.1 to 0.5  $\mu m$ . EDS microanalysis results (Table 2) show that silver content is  $\sim\!97-98\%$  in areas marked with  $\alpha 1,~\alpha 2,~\beta 1,~and~\beta 2.$  These areas also contain small amounts of Au and in some cases Pb and Sn in addition to lighter elements (Mg, Al, Ti, Si, O, Cl) with the total amount of  $\sim\!1\%$ .

The D5 and D7 coins have a similar near-surface microstructure with larger, irregular and slightly elongated pores. Such shape suggests that coin blanks were subjected to hammering, which led to elongation of Cu-rich grains. The selective leaching of copper created these directional pores. EDS microanalysis results for coin D5 (areas marked with  $\gamma$ ) indicating  $\sim\!95\%$  Ag,  $\sim\!1.5\%$  Cu and 1% Au along with lighter minor elements. For coin D7, a significant amount of sulfur was identified closer to the surface (point  $\pi1$ ). The  $\pi2$  area consists of 96% Ag as a major element, while remnants of gold were detected in the area closer to  $\pi3$ .

The SEM image of D11 coin exhibits significantly elongated pores revealing selective copper leaching, along with several deformed particles. These particles are primarily composed of Si and O ( $\delta$ 3) which could be slag, byproducts that have been attached to the surface of the blank coin that deformed and broke into smaller pieces during hammering. EDS microanalysis (areas marked with  $\delta 1$  and  $\delta 2$ ) shows that the alloy consists of 90–95% Ag, few percent Cu, some Au, and Pb as well as lighter elements.

Coin D14 exhibits both lighter Ag-rich (~85%) areas which contrast

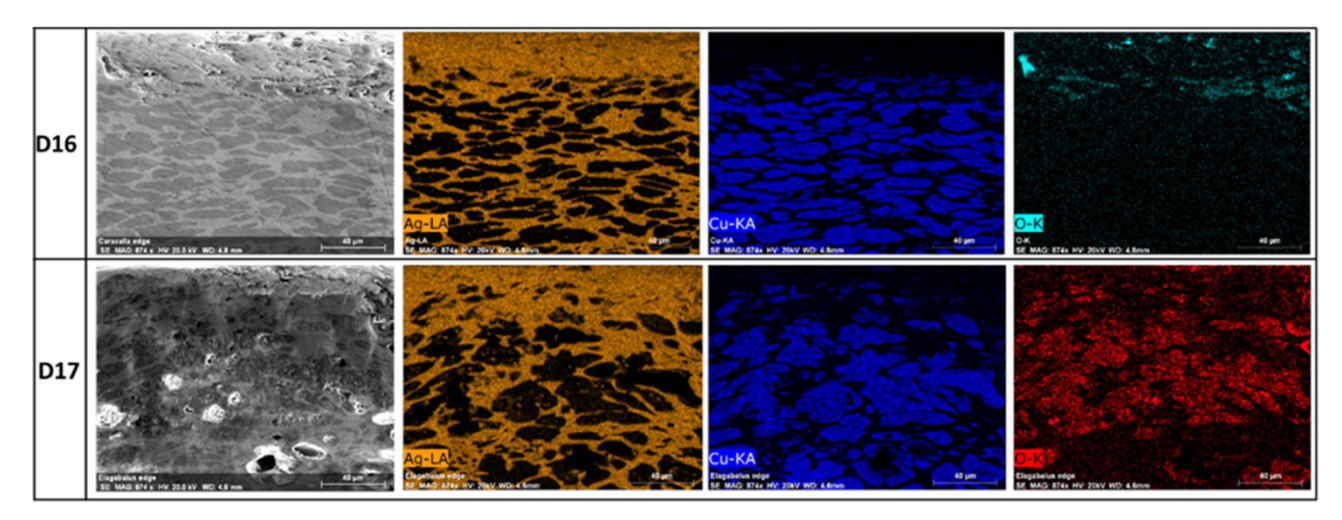


Fig. 7. EDS mapping of surface layers for two polished coins.

with darker areas composed of ~71% Cu, ~20% Ag, and additional minor elements. XRF and PIXE results indicated (Figs. 3 and 4) that D15 coin has the highest Cu content and exhibits non-uniform metal distribution Ag and Cu. Therefore, two different areas for this coin were investigated by the FIB-SEM-EDS method: a Cu-rich area on the coin center (see Fig. 3) and the Ag-rich area toward the edge. The two images, shown in Fig. 8, exhibit complex microstructures. The picture taken from the coin center shows Cu- (point  $\eta$ 1, Table 2) and Ag-rich (point  $\eta$ 2, Table 2) phases. The grains of these two phases are significantly elongated due to intensive working. Toward the coin edge, the surface layer exhibits a different microstructure with fine, brighter grains and darker inclusions. Microanalysis revealed that some light

grains contain  $\sim\!82\%$  Ag and  $\sim\!14\%$  Hg along with some other minor elements (point  $\eta 3$ , Table 2). The principal constituent of the phase with a darker contrast is copper (point  $\eta 4$ , Table 2). These results suggest that the amalgamation technique was used for developing a silver-rich surface layer on the debased Ag—Cu alloys. We can assume that this silver layer had poor adhesion to the alloy blank and was mostly removed during circulation.

The surface of coin D16 is highly porous, and the size of these pores can be as large as 5  $\mu$ m. The shape of the pores is irregular, and many of them are connected. The microanalysis in  $\kappa 1$  and  $\kappa 2$  areas (Table 2) reveal ~98% silver. The highly porous nature and high silver content suggest that there was selective leaching of Cu from the surface. The

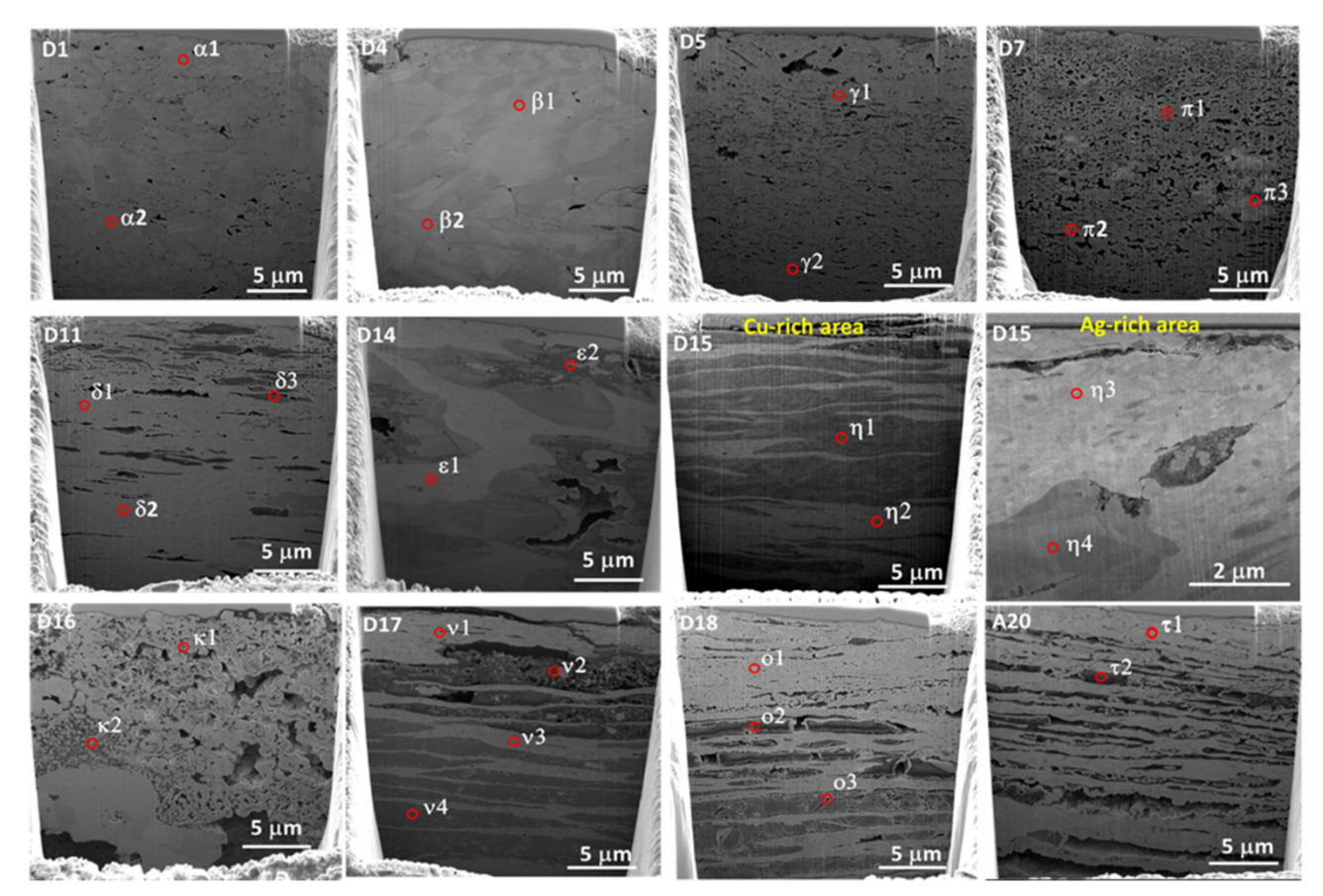


Fig. 8. FIB-SEM images of surface morphology of selected coins. The results of EDS analysis for the areas marked with Greek letters are summarized in Table 2.

**Table 2** EDS analysis results for the areas marked with Greek letters in Fig. 8. Experimental error is 1.0–2.0%.

Coin number	Area marked on Fig. 7	Ag	Cu	Au	Pb	Sn	Mg	Al	Ti	Fe	Hg	Si	O	S	Cl	P
D1	α1	97.68		1.23			0.26	0.26				0.22			0.35	
	α2	98.08		0.13	0.13	0.44	0.39	0.28	0.14			0.13			0.28	
D4	β1	97.36		1.15			0.67	0.22	0.4			0.08	0.12			
	β2	97.96		0.96		0.37	0.22					0.09	0.15		0.25	
D5	$\gamma 1$	95.76	1.53	1	0.11	0.38	0.46					0.11	0.31		0.34	
	$\gamma 2$	95.62	1.64	0.8			0.24		0.43			0.03	0.38	0.57	0.29	
D7	π1	89.36	3.73				0.46	0.43					0.87	4.59		0.56
	$\pi 2$	95.67	1.56	0.94			0.38		0.41				0.59	0.09	0.27	0.09
	π3	83.56	3.88	9.28		0.48	0.9		0.21				0.59	0.9	0.11	0.09
D11	δ1	94.4	2.81		0.83		0.56	0.16	0.32	0.61		0.13	0.18			
	δ2	90.94	4.68	1.03	0.22		1.58	0.2	1.01			0.06	0.28			
	δ3	71.32	2.95		0.25	0.18	0.53	0.15	0.11	0.64		17.1	6.77			
D14	ε1	85.31	11.8	1.19	0.4		0.33	0.24	0.47			0.03	0.23			
	ε2	20.1	71.29	2.45			0.58	0.07	0.15	0.79		0.04	4.53			
D15 Cu-rich area	η1	10.71	86.99	1.92					0.23				0.15			
	η2	82.06	15	1.18	0.51	0.27	0.39	0.11				0.34	0.14			
D15 Ag-rich area	η3	82.03	3.72	0.31	0.21						13.73					
	η4	13.41	80.97	1.59			0.66	0.05	0.26			0.04	3.02			
D16	κ1	98.06	0.48	0.88			0.05					0.4	0.13			
	κ2	98.07	0.22	0.76			0.34	0.14	0.34			0.04	0.09			
D17	$\nu 1$	90.95	6.1	0.79			0.62	0.29	0.19			0.67	0.39			
	$\nu 2$	47.19	43.17	1.94	0.17	0.37	0.47	0.02					6.36	0.31		
	ν3	87.99	8.94	0.91	0.18		1.05	0.18	0.24					0.51		
	ν4	16.14	77.7	1.75			1.24		0.14				3.03			
D18	o1	95.29	2.48	0.3		0.78	0.31	0.16				0.38	0.3			
	02	69.09	2.89	1.08			0.88	0.13	0.31			19.62	6			
	o3	60.41	29.75	3.41			2.81	1.01				0.89	1.72			
A20	τ1	97.07	1.15	0.31			0.5	0.11	0.37	0.24		0.06	0.19			
	τ2	85.23	3.52	0.64	0.17		0.45		0.24			7.04	2.71			

microstructure of coin D17 also indicates surface chemical enrichment by selective Cu leaching. In contrast to coin D16, the surface Ag-rich (see area  $\nu$ 1) layer has low porosity. However, some pores and Cu depleted areas ( $\nu$ 2) can be seen beneath this layer, which led to the local fracture of the Ag-rich surface layer during the striking. Below the modified surface layer, the coin exhibits double-phase morphology with Ag- ( $\nu$ 3) and Cu-rich ( $\nu$ 4) highly deformed grains.

The surface of D18 and A20 coins were also significantly enriched with Ag. Both of these coins exhibit elongated channel and some deformed slag inclusions, evidenced by local EDS analysis (areas o3 and  $\tau$ 2). The silver content in the enriched layer is above 95% (areas o1 and  $\tau$ 1). These results suggest that the coins were subjected to intensive silver enrichment by a selective Cu leaching approach.

## 3.5. TEM investigations

Two samples extracted from coins (D4 and D15) were analyzed by TEM to reveal their near-surface compositions. The sample for coin D15 was extracted from the silver-rich area toward the edge. Fig. 9 displays bright-field TEM images and selected area diffraction (SAD) patterns of samples as well as radial intensity diffraction profiles for samples taken from these two coins (Fig. 9). Intensity profiles were generated from SAD patterns described elsewhere [36,37]. TEM images and SAD patterns suggest that sample taken from D4 coin consists of larger grains compared to the one then taken from the Ag-rich area of coin D15. In both samples, randomly oriented grains show little or no deformation. The peaks on the diffraction profile of D4 can be indexed to pure silver, while the profile for coin D15 exhibits some other peaks that can be attributed to Cu-rich,  $Ag_3Hg$  phases or amalgam solid-solution.

Fig. 10 shows a high-angle annular dark-field (HAADF) image for the sample taken from coin D15. This imaging method is highly sensitive to variations of atomic number in the sample, and the heavier elements appear brighter in the image. The HAADF image shows both brighter and darker grains along with a porous area containing near spherical nanoparticles with 20–50 nm sizes. The high-resolution EDS spectrum indicates Cu as the principal constituent in a grain (area

marked as 1) with a darker contrast. The porous region of nanoparticles contains Cu, Pb, Ag, S, and O (area 2). The brighter area marked with 3 consists of Ag and some Hg. These investigations suggest that the amalgamation technique was used for developing a silver-rich surface layer on the debased Ag—Cu alloys.

## 4. Discussions

The scientific analysis of Roman coins reveals essential aspects of *the monetary system, alloy preparation*, and *corrosion processes* that are taking place over the long period. The results obtained in this work allow addressing several selected issues of these aspects.

The stability of the Roman monetary system was shaped by fiscal requirements, coin availability, market demand for metals, and a need to have an array of denominations suitable for a variety of transactions. It is common knowledge among numismatists and ancient historians that the Roman state would often manipulate the silver currency by adjusting the fineness and weight to cover fiscal deficits [10]. The first debasement of denarii was performed under the rule of Nero (54-68 CE) when the silver content was reduced to  $\sim$ 90%. Fig. 4 confirms the debasement by Nero in 65 CE (D5). The Cu amount remained rather constant during the subsequent century, with smaller fluctuation (Coin D8) that could be related to the debasements by Trajanus (98–117 CE). The increase and fluctuation of copper content at the end of the second century CE and the first 20 years of the third century CE provide evidence for the drastic devaluation established under Septimus Severus (D13-15), policies driven by the costs of maintaining the army and wars of expansion against the Germanic tribes and the Par-

An era of political unrest with the death of Septimius Severus increased inflation in the following years. These events are reflected in the fluctuation of the silver content of the coins (D15 and D16) minted under his sons and co-rulers, Geta (209–211 CE) and Caracalla (198–217 CE). After the murder of Geta, Caracalla became sole emperor. He developed a new taxation system, devalued the denarius to generate new revenue, and introduced the Antoninianus, a "double

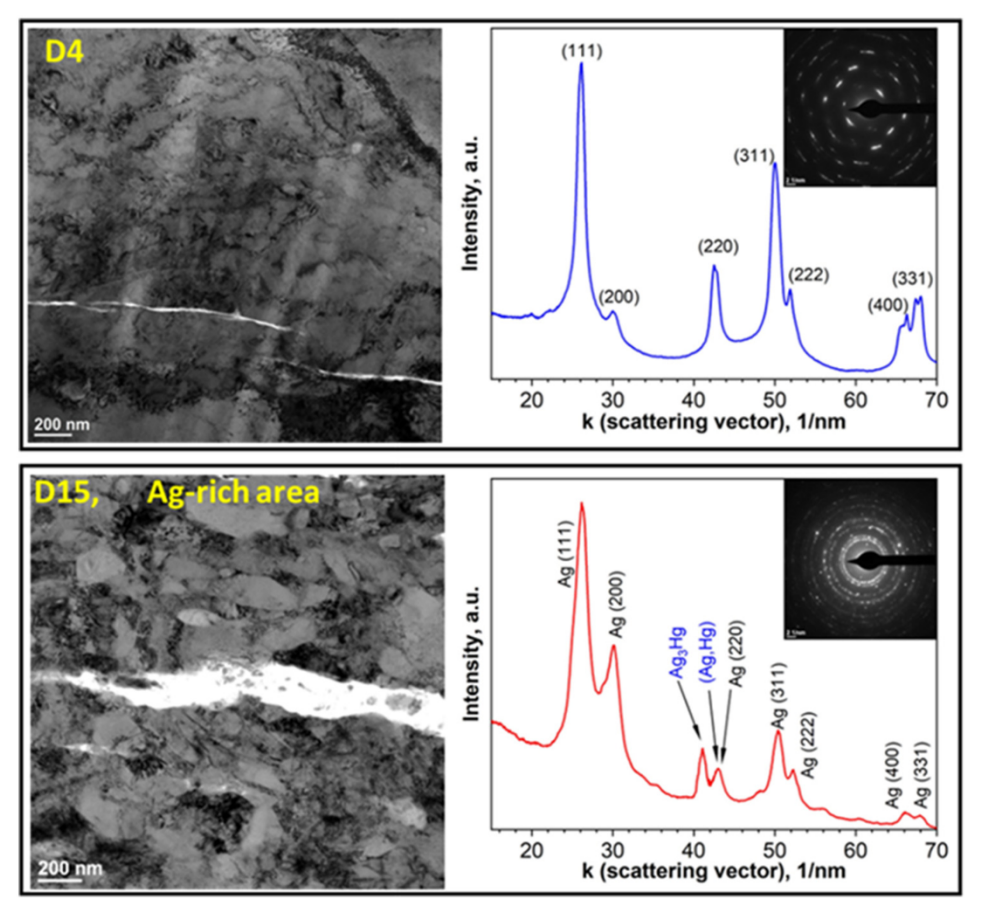


Fig. 9. TEM images, selected area diffraction (SAD) patterns of samples, as well as radial intensity profiles of diffraction patterns for samples taken from D4 and D15 coins.

Denarius." Elagabalus (218–222 CE) abandoned the Antoninianus but retained the debased standards of the Denarius (D17). During the relatively prosperous reign of Severus Alexander (222–235 CE) some brief stabilization of the currency took place (D18). The further debasement of coins by Maximinus Thrax (235–238 CE) led to a further decrease in the silver content (D19). Eventually, the denarius was replaced by the Antoninianus under Gordian III (238–244 CE), as the new standard silver currency (A20).

Another aspect of results obtained in this work is related to the surface treatment and corrosion of the coins. The degradation of similar silver coins has been reported in prior works [38-40,41]. Our results show that the corrosion mechanism depends on the chemical composition and surface treatment of alloys as well as on the environment in which the coins were and have been in contact. Coins minted during the republic and early imperial periods investigated in this work contain a small amount of copper. Cross-sectional SEM imaging suggests that coins minted during this period were subjected to limited treatment to enrich surface concentrator of Ag. Some of these coins, however, are heavily corroded. For example, Fig. 2 illustrates that the D2 coin exhibits area were the copper content is significantly higher. Optical and electron microscopy observation of this coin suggests that local deterioration originated at structurally inhomogeneous regions. These selectively corroded areas appear as green "islands" with dark red or black edges. Copper carbonate/hydroxyl carbonates (green color) or copper oxides (dark red or black) could be corrosion products for the copper-rich phase that reacts preferentially with pollutants at the surface [41]. Fig. 2 indicated that these areas also exhibit significant amounts of Fe. We can assume that exposed to a corrosive environment, such as burial soil components, created a difference in electrochemical potential between the different phases. The copper-rich structurally

inhomogeneous areas became as an anode and copper dissolve preferentially forming hydroxide and/or oxides. The reaction of these compounds with atmospheric carbon dioxide and water led to the formation of green copper carbonate or hydroxyl carbonates.

Another corrosion mechanism of coins minted in the republic and early imperial periods is mineralization, which could occur under the soil or sea. This is a relatively slow process and takes place continuously in halide (chloride- or bromine-rich) environments due to the high ionic mobility of silver. Figs. 2 and 3 indicate that D4 and D7 coins exhibit significant amounts of chlorine and bromine on the surface. XRD analysis of several coins proves that silver chloride is the main product of mineralization for such coins. We can suggest that in acidic soils relatively rapid preferential dissolution of the copper-rich phase generated imperfections. The presence of chloride or bromide salts resulted in the formation of silver halides over a much longer timescale. Neutral or basic soils with significant air-deficiency could also promote biodegradation of organic compounds to produce NH<sub>3</sub> and H<sub>2</sub>S. Release of H<sub>2</sub>S originated a new corrosion pathway resulting in silver sulfide. Figs. 2 and 3 clearly show the existence of such complex corrosion processes for D4 and D7 coins, which contain significant amounts of both halide and sulfur. We can assume such complex mineralization process involves different mass transfer processes. The silver undergoes outwards diffusion to form of Ag<sub>2</sub>S, while halide ions diffuse toward the core of the coin and replace silver. Such redistribution could create pores beneath the surface layer visible on cross-sectional SEM images for coins D1, D4, and D5 (Fig. 8). The TEM image of D15 coin (Fig. 10) also suggests the areas associated with high sulfur contents are porous and contain nanoparticles with 20-50 nm sizes. Such small Ag<sub>2</sub>S nanoscale particles are difficult to identify by XRD analysis (Fig. 5). Unlike Ag<sub>2</sub>S, silver chloride can be readily identified by XRD (Fig. 5).

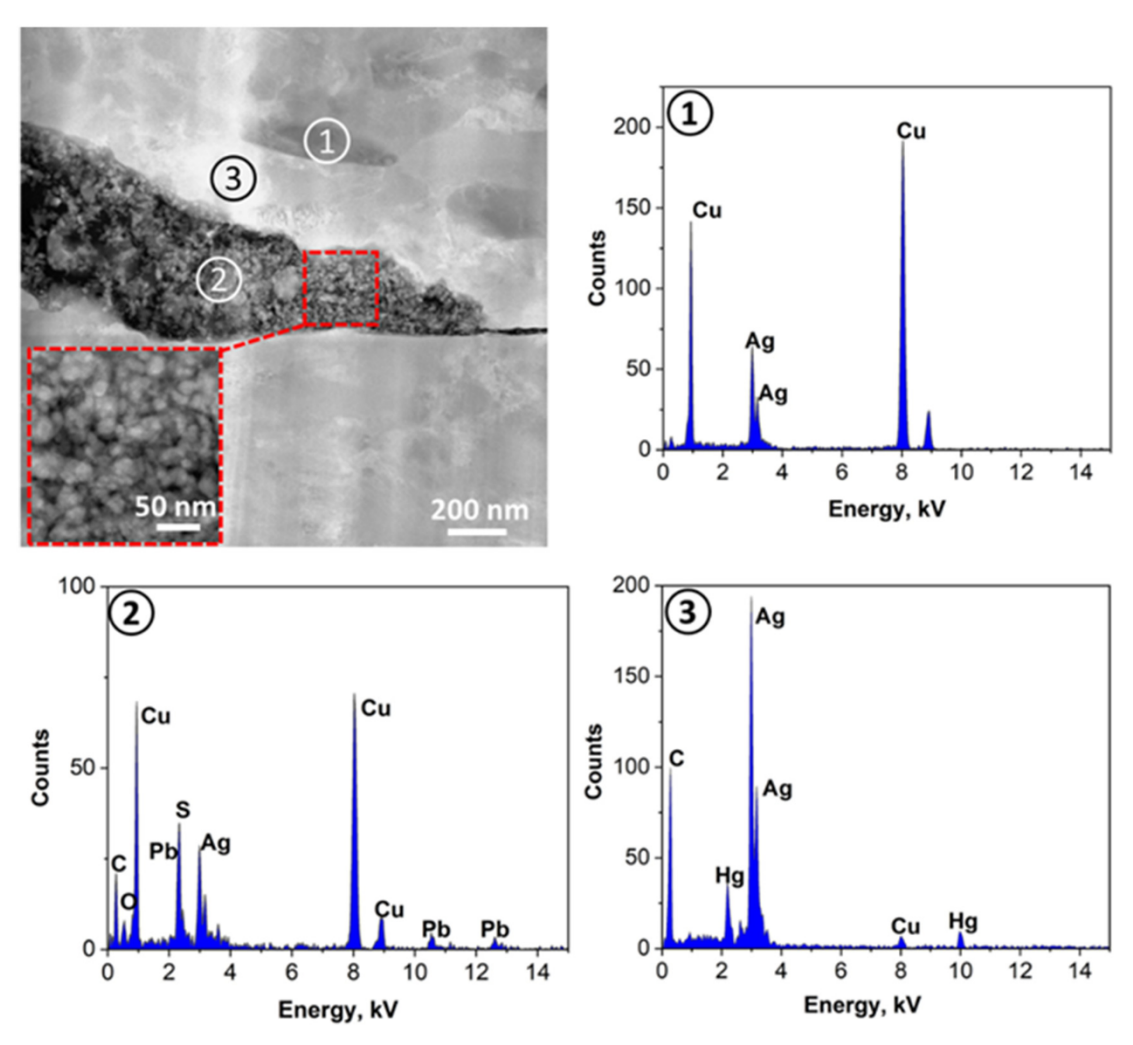


Fig. 10. HAADF image of the sample taken from the Ag-rich area of D15 coin and high-resolution EDS spectra for selected areas markers with 1, 2, and 3 numbers.

The degradation mechanism of copper-rich imperial coins (D10–D19, and A20) is different. Many of these coins show significant signs of surface treatment to enrich silver concentration. The use of organic acids, such as vinegar for dissolving the copper from the surface of the alloy created a thick (20–100  $\mu m$ ) porous copper-depleted layer. Copper residues after such treatment oxidized to form Cu<sub>2</sub>O surface phase (Figs. 5 and 7). Cross-sectional SEM images (Fig. 8) of copper-depleted layers indicate fractured areas due to their highly porous nature.

In some cases, sections of porous layers were detached, creating a non-uniform distribution of Ag and Cu (see Fig. 5). The surface silver-enriched layers of many coins contain highly deformed and fractured particles primarily composed of Si and O. These could be slag particles, byproducts that have been attached to the surface of the blank coins, which were severely deformed and fractured into smaller pieces during intense mechanical working. Substantial hammering is also evident form significantly elongated Ag- and Cu-rich grains and directional pores formed after soaking with organic solutions (Fig. 5).

The SEM and TEM imaging and local elemental analysis (Figs. 5 and 10) suggested that D15 coin contained a fragment of a thin Ag-rich surface layer with increased mercury concentrations. This fact indicates the use of amalgam silvering to produce a silver layer on coin blanks. The use of this method in the Roman Republic and Empire is a matter of debate, as highlighted in the Introduction section. Only several authentic coins are known, which indicate the use of mercury [17,38]. We can assume that the thin coatings produced by amalgam silvering were adhered weakly on the blank coins and readily detached form during

the circulation. This may explain why such surface modified coins were difficult to identify in prior works. Based on these investigations, we can suggest that the degradation patterns for D10–D19 and A20 coins are more complicated. The mechanical damage of the porous surface layer becomes an additional factor along with the selective corrosion and mineralization processes. The latter, however, is less pronounced in these coins. Future works should be directed for a better understanding of such complex corrosion mechanisms that involve mechanical damage and chemical degradation processes.

#### 5. Conclusions

A combination of XRF, PIXE, XRD, FIB-SEM-EDS, and TEM methods allows for the investigation of the surface, subsurface, and bulk composition of Roman coins. Such combinations of multiple techniques help in understanding the microstructural complexity of ancient silver coins and their manufacturing techniques as well as revealing essential degradation patterns. The results suggest that surface modification efforts for coins minted during the Roman Republic and early periods of the Roman Empire were minimal. The results also suggest that selective copper leaching was the primary method for surface manipulation during the second and third centuries. Based on obtained results, a few corrosion mechanisms were identified, which related to their chemical composition and the environment in which the coins have been in contact. These mechanisms involve selectively localized corrosion of copper as well as more complex mineralization that form silver halides and sulfide surface phases. Electron microscopy investigation suggests

that surface treatment results in the formation of the porous structure, which also contributes to the degradation of coins along with chemical corrosion. Electro microscopic observations, atomic level elemental analysis, disclose new evidence for the use of amalgam silvering during the early third century.

#### Acknowledgments

This work is supported by the Faculty Research Support Regular Grant program (FY17 FRSPC) of the University of Notre Dame. This work is also partially supported by the National Science Foundation under Grant No. PHY-1713857. C. Fasano and M. Raddell also acknowledge support from the Undergraduate Research Support Program from the College of Science, University of Notre Dame. The XRF and ICP analyses were conducted at the Center for Environmental Science and Technology (CEST) at the University of Notre Dame. Electron microscopy investigations were performed at Notre Dame Integrated Imaging Facility.

#### References

- D. Ashkenazi, H. Gitler, A. Stern, O. Tal, Metallurgical investigation on fourth century BCE silver jewellery of two hoards from Samaria, Sci. Rep. 7 (2017) 1–14, https://doi.org/10.1038/srep40659.
- [2] F.P. Romano, C. Caliri, L. Cosentino, S. Gammino, D. Mascali, L. Pappalardo, F. Rizzo, O. Scharf, H.C. Santos, Micro X-ray fluorescence imaging in a tabletop full field-X-ray fluorescence instrument and in a full field-particle induced X-ray emission end station, Anal. Chem. 88 (2016) 9873–9880, https://doi.org/10.1021/acs. analchem.6b02811.
- [3] A. Doménech-Carbó, M.T. Doménech-Carbó, M.A. Peiró-Ronda, Dating archeological lead artifacts from measurement of the corrosion content using the voltammetry of microparticles, Anal. Chem. 83 (2011) 5639–5644, https://doi.org/10. 1021/ac2007310.
- [4] M.T. Doménech-Carbó, F. Di Turo, N. Montoya, F. Catalli, A. Doménech-Carbó, C. De Vito, FIB-FESEM and EMPA results on Antoninianus silver coins for manufacturing and corrosion processes, Sci. Rep. 8 (2018) 1–12, https://doi.org/10.1038/s41598-018-28990-x.
- [5] A. Giumlia-Mair, C. Albertson, G. Boschian, G. Giachi, P. Iacomussi, P. Pallecchi, G. Rossi, A.N. Shugar, S. Stock, Surface characterisation techniques in the study and conservation of art and archaeological artefacts: a review, Mater. Technol. 25 (2010) 245–261, https://doi.org/10.1179/175355510X12850784228001.
- [6] C.J. Keturakis, B. Notis, A. Blenheim, A.C. Miller, R. Pafchek, M.R. Notis, I.E. Wachs, Analysis of corrosion layers in ancient Roman silver coins with high resolution surface spectroscopic techniques, Appl. Surf. Sci. 376 (2016) 241–251, https://doi.org/10.1016/j.apsusc.2016.03.009.
- [7] L. Kučera, L. Richtera, M. Zmrzlý, M. Jarošová, P. Kučerová, P. Bednář, Determination of the fineness of medieval coins—evaluation of methods in a case study of a medieval pfennig, Archaeometry 60 (2018) 325–341, https://doi.org/10. 1111/arcm.12313.
- [8] G.M. Ingo, G. Guida, E. Angelini, G. Di Carlo, A. Mezzi, G. Padeletti, Ancient mercury-based plating methods: combined use of surface analytical techniques for the study of manufacturing process and degradation phenomena, Acc. Chem. Res. 46 (2013) 2365–2375, https://doi.org/10.1021/ar300232e.
- [9] K.W. Harl, Coinage in the Roman Economy, 300 B.C to A.D. 700, John Hopkins University Press, Baltimore & London, 1996.
- [10] K. Butcher, M. Ponting, J. Evans, V. Pashley, C. Somerfield, The Metallurgy of Roman Silver Coinage: From the Reform of Nero to the Reform of Trajan, Cambridge University Press, 2015, https://doi.org/10.1017/CBO9781139225274.
- [11] G. Sarah, B. Gratuze, J.N. Barrandon, Application of laser ablation inductively coupled plasma mass spectrometry (LA-ICP-MS) for the investigation of ancient silver coins, J. Anal. At. Spectrom. 22 (2007) 1163–1167, https://doi.org/10.1039/ b704879c.
- [12] L. Beck, E. Alloin, C. Berthier, S. Réveillon, V. Costa, Silver surface enrichment controlled by simultaneous RBS for reliable PIXE analysis of ancient coins, Nucl. Instruments Methods Phys. Res. Sect. B Beam Interact. with Mater. Atoms. 266 (2008) 2320–2324, https://doi.org/10.1016/j.nimb.2008.03.084.
- [13] F.J. Ager, A.I. Moreno-Suárez, S. Scrivano, I. Ortega-Feliu, B. Gómez-Tubío, M.A. Respaldiza, Silver surface enrichment in ancient coins studied by micro-PIXE, Nucl. Instruments Methods Phys. Res. Sect. B Beam Interact. with Mater. Atoms. 306 (2013) 241–244, https://doi.org/10.1016/j.nimb.2012.12.037.
- [14] L. Beck, S. Besonnet, S. Réveillon, D. Eliot, F. Pilon, Silver surface enrichment of silver-copper alloys: a limitation for the analysis of ancient silver coins by surface techniques, Nucl. Instruments Methods Phys. Res. Sect. B Beam Interact. with Mater. Atoms. 226 (2004) 153–162, https://doi.org/10.1016/S0168-583X(04) 00831-6.
- [15] K. Anheuser, Where is all the amalgam silvering? Mater. Issues Art Archaeol. V Symp. Held December 3–5, 1996, Boston, Massachusetts, USA, 1996, pp. 127–134, , https://doi.org/10.1557/PROC-462-127.
- [16] C. Vlachou, J.G. McDonnell, R.C. Janaway, Experimental investigation of silvering in late Roman coinage, Mater. Issues Art Archaeol. VI Symp. Held Novemb. 26–30, 2001, Boston, Massachusetts, USA, 2002, pp. 461–469, https://doi.org/10.1557/ PROC-712-II9.2.

- [17] G.M. Ingo, C. Riccucci, F. Faraldi, M. Pascucci, E. Messina, G. Fierro, G. Di Carlo, Roman sophisticated surface modification methods to manufacture silver counterfeited coins, Appl. Surf. Sci. 421 (2017) 109–119, https://doi.org/10.1016/j. apsusc.2017.01.101.
- [18] A. Deraisme, L. Beck, F. Pilon, L. Niece, A study of the silvering process of the gallo-Roman coins forged during the third century AD, Archaeometry 3 (2006) 469–480.
- [19] J. Corsi, B. Maróti, A. Re, Z. Kasztovszky, L. Szentmiklósi, M. Torbágyi, A. Agostino, D. Angelici, S. Allegretti, Compositional analysis of a historical collection of Cisalpine Gaul's coins kept at the Hungarian National Museum, J. Anal. At. Spectrom. 30 (2015) 730–737, https://doi.org/10.1039/c4ja00398e.
- [20] J. Lekki, M. Matosz, C. Paluszkiewicz, E. Pięta, T. Pieprzyca, Z. Szklarz, J.M. del Hoyo Meléndez, Comparison of PIXE and XRF in the analysis of silver denarii of the early Piast, J. Radioanal. Nucl. Chem. 314 (2017) 2309–2316, https://doi.org/10. 1007/s10967-017-5556-8.
- [21] S. Pessanha, M. Costa, M.I. Oliveira, M.E.M. Jorge, M.L. Carvalho, Nondestructive analysis of Portuguese "dinheiros" using XRF: overcoming patina constraints, Appl. Phys. A Mater. Sci. Process. 119 (2015) 1173–1178, https://doi.org/10.1007/ s00339-015-9087-2.
- [22] M. Scuotto, C. Bassi, M. Lezzerini, E. Grifoni, S. Legnaioli, G. Lorenzetti, S. Pagnotta, V. Palleschi, X-ray fluorescence analysis on a group of coins from the ancient roman city of Tridentum (Trento, Italy), X-Ray Spectrom. 43 (2014) 370–374, https://doi. org/10.1002/xrs.2567.
- M.W. Hinds, G. Bevan, R.W. Burgess, The non-destructive determination of Pt in ancient Roman gold coins by XRF spectrometry, J. Anal. At. Spectrom. 29 (2014) 1799–1805, https://doi.org/10.1039/c4ja00170b.
   M.E. Fedi, L. Caforio, P.A. Mandò, F. Petrucci, F. Taccetti, Nuclear Instruments and
- [24] M.E. Fedi, L. Caforio, P.A. Mandò, F. Petrucci, F. Taccetti, Nuclear Instruments and Methods in Physics Research B, Nucl. Inst. Methods Phys. Res. B 294 (2013) 662–665, https://doi.org/10.1016/j.nimb.2009.08.026.
- [25] F. Caridi, L. Torrisi, M. Cutroneo, F. Barreca, C. Gentile, T. Serafino, D. Castrizio, XPS and XRF depth patina profiles of ancient silver coins, Appl. Surf. Sci. 272 (2013) 82–87, https://doi.org/10.1016/j.apsusc.2012.02.071.
- [26] F.P. Romano, S. Garraffo, L. Pappalardo, F. Rizzo, In situ investigation of the surface silvering of late Roman coins by combined use of high energy broad-beam and low energy micro-beam X-ray fluorescence techniques, Spectrochim. Acta B At. Spectrosc. 73 (2012) 13–19, https://doi.org/10.1016/j.sab.2012.05.012.
- [27] F. Rizzo, G.P. Cirrone, G. Cuttone, A. Esposito, S. Garraffo, G. Pappalardo, L. Pappalardo, F.P. Romano, S. Russo, Non-destructive determination of the silver content in Roman coins (nummi), dated to 308–311 A.D., by the combined use of PIXE-alpha, XRF and DPAA techniques, Microchem. J. 97 (2011) 286–290, https:// doi.org/10.1016/j.microc.2010.09.017.
- [28] A. Gianoncelli, G. Kourousias, Limitations of portable XRF implementations in evaluating depth information: an archaeometric perspective, Appl. Phys. A Mater. Sci. Process. 89 (2007) 857–863, https://doi.org/10.1007/s00339-007-4221-4.
- [29] M. Cutroneo, L. Torrisi, F. Caridi, R. Sayed, C. Gentile, G. Mondio, T. Serafino, E.D. Castrizio, Silver/oxygen depth profile in coins by using laser ablation, mass quadrupole spectrometer and X-rays fluorescence, Appl. Surf. Sci. 272 (2013) 25–29, https://doi.org/10.1016/j.apsusc.2012.03.133.
- [30] L. Pardini, A. El Hassan, M. Ferretti, A. Foresta, S. Legnaioli, G. Lorenzetti, E. Nebbia, F. Catalli, M.A. Harith, D. Diaz Pace, F. Anabitarte Garcia, M. Scuotto, V. Palleschi, X-ray fluorescence and laser-induced breakdown spectroscopy analysis of Roman silver denarii, Spectrochim. Acta B At. Spectrosc. 74–75 (2012) 156–161, https://doi.org/10.1016/j.sab.2012.06.016.
- [31] F.J. Ager, B. Gómez-Tubío, A. Paúl, A. Gómez-Morón, S. Scrivano, I. Ortega-Feliu, M.A. Respaldiza, Combining XRF and GRT for the analysis of ancient silver coins, Microchem. J. 126 (2016) 149–154, https://doi.org/10.1016/j.microc.2015.12. 017.
- [32] M. Rodrigues, F. Cappa, M. Schreiner, P. Ferloni, M. Radtke, U. Reinholz, B. Woytek, M. Alram, Further metallurgical analyses on silver coins of Trajan (AD 98–117), J. Anal. At. Spectrom. 26 (2011) 984–991, https://doi.org/10.1039/ c0ja00252f.
- [33] J.A. Maxwell, W.J. Teesdale, J.L. Campbell, Ifi the Guelph PIXE software package II, Nucl. Inst. Methods Phys. Res. B 95 (1995) 407–421.
- [34] G.M. Ingo, C. Riccucci, M. Pascucci, E. Messina, C. Giuliani, G. Fierro, G. Di Carlo, Integrated analytical methodologies for the study of the corrosion products naturally grown on Roman Ag-based artefacts, Appl. Surf. Sci. 446 (2018) 279–286, https://doi.org/10.1016/j.apsusc.2017.11.066.
- [35] T.B. Massalski, H. Okamoto, P.R. Subramanian, L. Kacprzak (Eds.), Binary Alloy Phase Diagrams, 2nd edition, ASM International, 1990.
- [36] J.L. Lábár, Electron diffraction based analysis of phase fractions and texture in nanocrystalline thin films, part I: principles, Microsc. Microanal. 14 (2008) 287–295, https://doi.org/10.1017/S1431927609090023.
- [37] J.L. Lábár, Consistent indexing of a (set of) single crystal SAED pattern(s) with the process diffraction program, Ultramicroscopy 103 (2005) 237–249, https://doi. org/10.1016/j.ultramic.2004.12.004.
- [38] G.M. Ingo, E. Angelini, T. De Caro, G. Bultrini, Combined use of surface and microanalytical techniques for the study of ancient coins, Appl. Phys. A Mater. Sci. Process. 79 (2004) 171–176, https://doi.org/10.1007/s00339-004-2510-8.
- [39] G. Giovannelli, S. Natali, B. Bozzini, A. Siciliano, G. Sarcinelli, R. Vitale, Microstructural characterization of early western Greek incuse coins, Archaeometry 47 (2005) 817–833.
- [40] R. Borges, L. Alves, R.J.C. Silva, M.F. Araújo, A. Candeias, V. Corregidor, P. Valério, P. Barrulas, Investigation of surface silver enrichment in ancient high silver alloys by PIXE, EDXRF, LA-ICP-MS and SEM-EDS, Microchem. J. 131 (2017) 103–111, https://doi.org/10.1016/j.microc.2016.12.002.
- [41] L. Fabrizi, F. Di Turo, L. Medeghini, M. Di Fazio, F. Catalli, C. De Vito, The application of non-destructive techniques for the study of corrosion patinas of ten Roman silver coins: the case of the medieval Grosso Romanino, Microchem. J. 145 (2019) 419–427, https://doi.org/10.1016/j.microc.2018.10.056.